energies

MDPI

*Article*

# High Efficiency of the Removal Process of Pb(II) and Cu(II) Ions with the Use of Fly Ash from Incineration of Sunflower and Wood Waste Using the CFBC Technology

**Tomasz Kalak [1,*], Ryszard Cierpiszewski [1] and Małgorzata Ulewicz [2]**

[1] Department of Industrial Products and Packaging Quality, Institute of Quality Science, Poznań University of Economics and Business, Niepodległości 10, 61-875 Poznań, Poland; ryszard.cierpiszewski@ue.poznan.pl
[2] Faculty of Civil Engineering, Częstochowa University of Technology, Akademicka 3 Street, 42-200 Częstochowa, Poland; malgorzata.ulewicz@pcz.pl
* Correspondence: tomasz.kalak@ue.poznan.pl

**Abstract:** In these research studies, fly ash (SW-FA) resulting from the incineration of sunflower (20%) and wood (80%) waste employing the circulating fluidized bed combustion (CFBC) technology was used to analyze the possibility of removing Pb(II) and Cu(II) ions in adsorption processes. Currently, great emphasis is placed on circular economy, zero waste or climate neutrality strategies. The use of low-cost SW-FA waste seems to fit well with pro-ecological, economic and energy-saving trends. Hence, this material was characterized by various techniques, such as granulation analysis, bulk density, SEM-EDX, XRD and XRF analysis, BET, BJH, thermogravimetry, zeta potential, SEM morphology and FT-IR spectrometry. As a result of the conducted research, the factors influencing the effectiveness of the adsorption process, such as adsorbent dosage, initial and equilibrium pH, initial metal concentration and contact time, were analyzed. The maximum removal efficiency were achieved at the level of 99.8% for Pb(II) and 99.6% for Cu(II), respectively. The kinetics analysis and isotherms showed that the pseudo-second-order equation and the Freundlich isotherm models better describe these processes. The experiments proved that SW-FA can act as an appropriate adsorbent for highly effective removal of lead and copper from wastewater and improvement of water quality.

**Keywords:** water quality; cleaner environment; waste management; removal efficiency; fly ash from sunflower and wood residues; Pb(II) and Cu(II) ions; kinetics



**Citation:** Kalak, T.; Cierpiszewski, R.; Ulewicz, M. High Efficiency of the Removal Process of Pb(II) and Cu(II) Ions with the Use of Fly Ash from Incineration of Sunflower and Wood Waste Using the CFBC Technology. *Energies* **2021**, *14*, 1771. https://doi.org/10.3390/en14061771

Academic Editor: Artur Błaszczuk

Received: 26 January 2021
Accepted: 19 March 2021
Published: 23 March 2021



## 1. Introduction

In recent years, many global problems related to the aquatic environment have been observed, such as water waste, the presence of industrial and consumer waste in oceans, and pollution by heavy metals and other toxic substances. The frequency of these phenomena is increasing and they hinder assumptions of sustainable economic development. Individual responsibility for environmental degradation is difficult to establish, so collective responsibility should be seen in the consumer, industrial and system spheres [1]. Heavy metals pollute the aquatic environment through human activities and are particularly dangerous because they are not biodegradable and accumulate in the ecosystem through food chains. Accumulating in living organisms and humans, even in low concentrations, they can cause diseases of various organs and systems and with longer exposure, can even lead to loss of life [2].

One of the most toxic metals is lead (Pb). Many studies in the literature have shown its damaging effects on the kidneys and its involvement in diseases of the cardiovascular, nervous and musculoskeletal systems and hormonal imbalance [3]. Additionally, the International Agency for Research on Cancer has classified inorganic lead compounds to Group 2A and organic lead compounds remain in Group 3, which means they have

carcinogenic effects on the human body [4]. Another toxic metal that has a negative effect on the environment and human health is copper (Cu). This element in high concentrations damages cells in living organisms and leads to many diseases, such as haemolysis, hepatotoxic and nephrotoxic effects, Wilson's disease, extensive damage to the capillaries and the central nervous system [5]. Additionally, copper causes many harmful and toxic effects by accumulating in the liver, brain, pancreas and heart muscle. Inhaling copper vapors may cause dizziness, headaches, irritation, upset stomach, diarrhea and vomiting [6,7]. Copper is the most toxic in the form of divalent Cu(II) metal and it is mainly found in industrial waste and sewage. This ionic form is able to dissolve in water and be absorbed by living organisms. In accordance with World Health Organisation (WHO), the maximum limits in drinking water are 0.015 mg/L for lead (Pb) and 2 mg/L for copper (Cu). Moreover, the United States Environmental Protection Agency (USEPA) has set the maximum level of contamination (MCL) at the level of 0.015 mg/L for Pb and 1.3 mg/L for Cu [8,9]. Thus, the removal of Pb(II) and Cu(II) from the aquatic environment is an important global problem.

Currently, many expensive and advanced technologies are used to treat wastewater contaminated with metals, such as adsorption, ion exchange, chemical precipitation, ultrafiltration, electrolysis, reverse osmosis [10]. Unfortunately, their investment and operating costs are very high, therefore cheaper solutions and innovative technologies are constantly being sought. One of them is undoubtedly the adsorption process, which is characterized by low costs, ease of operation, no requirements for expensive and modern equipment and apparatus, the possibility of application to various types of pollutants [11]. A great advantage is the possibility of using low-cost industrial, agricultural and municipal waste for heavy metal removal processes. The adsorption of metals was investigated using various biomaterials, such as: orange biomass [12], fruit peel of orange [13], dried plants [14], miscanthus [15], potato peel [16], pectin gel [17], cow dung [18], waste leaves biomass of *Myrica esculenta* [19]. These materials contain various valuable components and functional groups, such as amine, carboxyl, hydroxyl, carbonyl capable of binding metal cations [20]. One of the most commonly used adsorbents is fly ash (FA) produced from various wastes and materials [21–24].

The study on FA adsorption has been performed for many heavy metals, including copper and lead. Buema et al. used FA generated from a power plant with different systems. According to the presented data, the FA exhibits adsorption capacity for Cu(II) ions equal to 27.32–58.48 mg/g [25]. Wu et al. presented the maximum adsorption capacity for Cu(II) at the level of 48.8 mg/g [26]. Kumar et al. analyzed the possibility of removal of Cd(II), Ni(II), Cu(II) in aqueous systems. The maximum sorption was achieved at initial concentration of 10 mg/L [27]. FA generated from municipal solid waste incineration (MSWI) was used for metal adsorption processes in landfill leachate.The optimal dosage of FA was 10 g/L and removal efficiency of Pb(II), Cu(II) Zn(II), Cd(II) and Cr(III) was achieved at the level of 59.24, 32.82, 39.42, 55.37 and 28.14%, respectively [28]. FA collected as solid waste material from a power plant was examined for Pb(II) sorption. Within the scope of the examined variables, the percentage of adsorption changed from 68.39% to 91.89% [29].

Pursuant to the Polish Regulation of the Minister of the Environment of 9 December 2014 concerning the catalogue of waste (Journal of Laws of 2014, item 1923), FA from biomass incineration in fluidized bed boilers is classified into the same group of waste as the byproducts of conventional fuel combustion, i.e., group 10 01 01—including slag, bottom ash and boiler dust (apart from boiler dust mentioned in 10 01 04) and to group 10 01 24 containing fluidized bed sands (except 10 01 82). The subject of interest in this article is fluidized FA obtained in the combustion process of sunflower and wood waste. Globally and in Poland, FA from the combustion of biomass alone is tested usually in laboratories, however, they have no practical use. Especially, FA from the process of biomass co-combustion with coal has practical application, e.g., in construction for the production of ceramic materials, construction binders and land filling. Currently, the energy sector in Europe produces over 150 million tons of coal combustion by-products annually,

of which over 100 million tons are generated in 28 Member States of the European Union, and 480 million tons in the world [30,31]. In Poland, about 15 million tons of energy FA and slag and about 5 million tons of gypsum from flue gas desulphurization are produced every year. In addition, other combustion by-products are produced, such as waste from lime flue gas desulfurization methods, sludge, fluidized bed sands and FA-slag mixtures from wet furnace waste discharge. It is estimated that the total amount of combustion by-products currently produced in the country amounts to approximately 23 million tons per year [32].

A large scale of sunflower production in 2020/2021 takes place in a limited number of countries, i.e., as much as two-thirds of production is located in European Union (9.2 million tons), including Ukraine (14 Mt), Russia (13 Mt) and the Trakya region in Turkey (1.56 Mt). The other main producers are as follows: China (3.3 Mt), Argentina (2.9 Mt), the United States (1.273 Mt) and others (Figure 1). According to the United States Department of Agriculture (USDA), in 2020 global sunflower production was equal to 54.96 million tons with a cultivation area of about 26 million hectares [33,34].

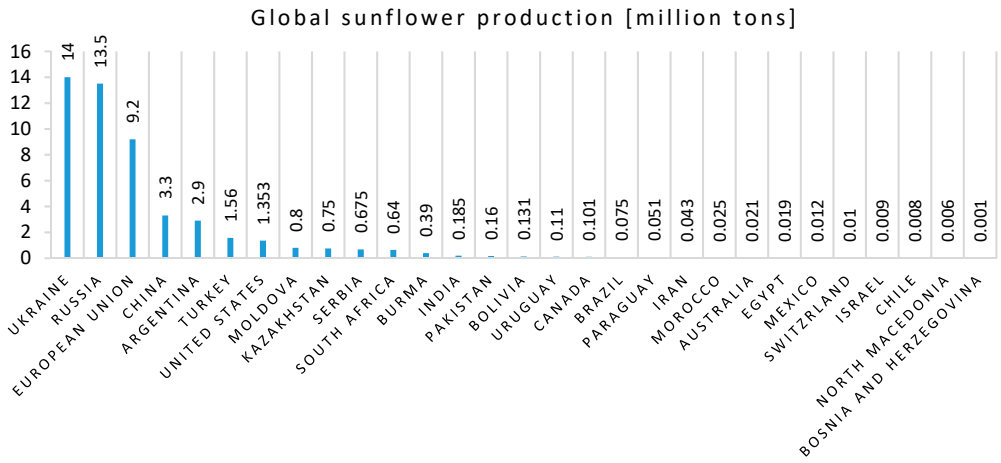


**Figure 1.** Global sunflower production 2020/2021 based on the United States Department of Agriculture (USDA) [33].

Sunflower is usually grown for its fruit (seeds) for human and farm animal consumption, but also for the edible oil. About 21–30% of the total weight of seeds are shell sunflowers, so their annual production is in the range of about 9.45–13.5 million tons per year [35]. On the other hand, about 3964.3 million $m^3$ roundwood production worldwide was recorded in 2019 (Figure 2) [36]. The total waste from industrial wood production in 2013 was estimated at around 715 million tons. Among the countries generating the most wood waste, the following ones can be distinguished: USA (155.8 Mt), Russia (95.5 Mt), Brazil (82.3 Mt), Canada (78.4 Mt), China (77.2 Mt), Poland (17.4 Mt) and others (Figure 3) [37]. Wood waste is mainly sourced from a variety of sources, such as wood packaging, demolition and construction activity, the wood industry, municipal waste, imported wood and others, e.g., private households and railroad construction [38]. In accordance with the literature, approximately 25–30% of the total weight of processed fruit, vegetables and other plant raw materials is waste from the food industry [39]. This huge amount of waste needs to be recycled and an alternative could be to incinerate it to reduce waste weight and produce FA. One potential application of FA from incineration of sunflower and wood waste could be the use in adsorption processes to remove metal ions from wastewater and improvement of water quality and the purity of aquatic environment.

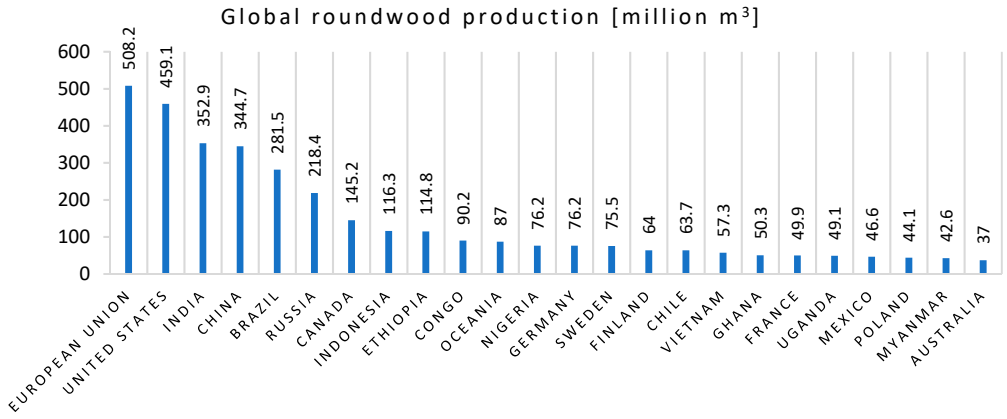


**Figure 2.** Global roundwood production 2019 based on Undata [36].


**Figure 3.** Global residue from industrial wood production [37].

The purpose of these studies was to examine the possibility of Pb(II) and Cu(II) ions removal from water using fly ash obtained from the incineration of sunflower (20%, *m/m*) and wood (80%, *m/m*) waste in the circulating fluidized bed combustion (CFBC) technology under different conditions of adsorbent dosage, initial and equilibrium pH, initial concentration and contact time. Additionally, the goal was to determine physico-chemical properties of the material and to study adsorption kinetics, equilibrium and isotherms.

## 2. Experimental Procedure

### *2.1. Materials and Methods*

#### 2.1.1. Sunflower Wood Fly Ash Preparation

The sunflower wood fly ash (SW-FA) used in this research was produced in one of waste incineration plants located in Poland (Świętokrzyskie voivodeship, Połaniec, Poland) in the process of burning sunflower (20%, *m/m*) and wood (80%, *m/m*) waste in the circulating fluidized bed combustion (CFBC) technology. This power plant has the largest power unit in the world that uses 100% biomass combustion. Fluidized bed boilers are the most modern types of boilers characterized by the highest operating parameters and the best efficiency during the combustion process, reaching over 80%. The fuel in these boilers is burnt in a suspended form, therefore it must be finely fragmented. The suspended form is obtained by selecting an appropriate air flow velocity through the combustion chamber in such a way that it is greater than the falling velocity of fuel particles and additional inert material. The fluidized boiler has a bed, natural circulation, and a three-pass secondary superheat. The technological parameters of the boiler are as follows: live steam pressure 127.5 bar, the pressure of the re-superheated steam 19.5 bar, live steam temperature 535 °C, the temperature of the re-superheated steam 535 °C, supply water temperature 242 °C, live steam flow 158 kg/s (570 t/h), re-superheated steam flow 135 kg/s (486 t/h). The

gas emissions from combustion are as follows: NOx 150 mg/m$^3$n, $SO_2$ 150 mg/m$^3$n, CO 50 mg/m$^3$n, particular matter 20 mg/m$^3$n. The combustion efficiency in the fluidized bed boiler is 220,000 tons of biomass and 900,000 tons of wood waste per year. The generated heat energy in the power plant is converted into electricity, which amounts to 1.2 TWh per year. Samples of SW-FA were taken from the boiler after the combustion process. Firstly, four SW-FA samples were collected from different places in the tank, and then combined into one sample and mixed. Then, samples were taken from the averaged mass for all analyzes. Next, SW-FA was sieved and particles with a diameter in the range 0–0.212 mm were taken for analysis. The samples were dried at 105 °C to constant weight (the moisture content was less than 0.2%) and stored in an desiccator (Figure 4). In this research, distilled water and chemical reagents were analytically pure.

**Figure 4.** Sunflower wood fly ash after the drying process.

#### 2.1.2. Sunflower Wood Fly Ash Characterization

In the research, sunflower wood fly ash (SW-FA) particles with a diameter in the range of 0–0.212 mm were used. Firstly, physical and chemical properties of the material were analyzed using several methods, such as: granulation analysis, bulk density, the elemental composition and mapping using SEM-EDX analysis, XRD, XRF, specific surface area and pore volume (BET, BJH), thermogravimetry, electrokinetic zeta potential, SEM morphology, FT-IR spectrometry. The description of the research methods and apparatus has been attached to this article as Supplementary Materials (SM Methods).

#### 2.1.3. Pb(II) and Cu(II) Adsorption Process

SW-FA was examined for the possibility of the adsorption of Pb(II) and Cu(II) ions in aqueous solutions at room temperature (23 ± 1 °C). For this purpose, $Pb(NO_3)_2$ and $CuCl_2$ with analytical purity were applied. The SW-FA samples (weight from 20 to 100 mg) and $Pb(NO_3)_2$ or $CuCl_2$ solution (V = 20 mL, concentration ranged from 20 to 100 mg/L) at pH 2–5 were added to conical flasks and mechanically shaken at 200 rpm (1 h) until the equilibrium phase. The pH of Pb(II) and Cu(II) initial solutions was adjusted with 0.1 M $HNO_3$ and NaOH. Next, the SW-FA and equilibrium solution phases were separated by centrifugation at 4000 rpm. Subsequently, the concentration of Pb(II) and Cu(II) ions [mg/L] was analyzed using a SpectrAA 800 atomic absorption spectrophotometer (F-AAS, at a wavelength λ = 217 nm for lead Pb and λ = 324.8 nm for copper Cu, Varian, Palo Alto, CA, USA). The measurements were conducted in triplicate and average results were finally presented.

According to the Equations (1) and (2), the adsorption efficiency $A$ [%] and adsorption capacity $q_e$ [mg/g] were evaluated, respectively:

$$A = \left[\frac{C_0 - C_e}{C_0}\right] \times 100\% \quad (1)$$

$$q_e = \frac{(C_0 - C_e) \times V}{m} \quad (2)$$

where: $C_0$ and $C_e$ [mg/L] are initial and equilibrium metal ion concentrations, respectively; $V$ [L]—volume of solution, $m$ [g]—mass of SW-FA.

Langmuir, Freundlich, pseudo-first-order and pseudo-second-order models were used for analysis according to the Equations (3)–(6), respectively:

$$q_e = \frac{q_{max} K_L C_e}{1 + K_L C_e} \tag{3}$$

$$q_e = K_F C_e^{\frac{1}{n}} \tag{4}$$

$$q_t = q_e\left(1 - e^{k_1 t}\right) \tag{5}$$

$$q_t = \frac{q_e^2 k_2 t}{1 + q_e k_2 t} \tag{6}$$

where: $K_L$—the Langmuir constant; $q_{max}$ [mg/g]—the maximum adsorption capacity; $C_e$ [mg/L]—the equilibrium concentration after the adsorption process; *1/n*—the intensity of adsorption; $K_F$—the Freundlich constant, $q_t$ [mg/g]—the amount of Pb(II) or Cu(II) ions adsorbed at any time $t$ [min]; $q_e$ [mg/g]—the maximum amount of Pb(II) or Cu(II) ions adsorbed per mass of SW-FA at equilibrium; $k_1$ [1/min]—the rate constant of pseudo-first-order adsorption; $k_2$ [g/(mg·min.)]—the rate constant of pseudo-second-order adsorption.

## 3. Results and Discussion

### *3.1. Characterization of the Adsorbent*

In these research studies, the sunflower wood fly ash has been analysed using several methods. Based on the granulation analysis, the following grain diameter fractions were identified: 0–0.212 mm (90.93 ± 1.5%), 0.212–0.5 mm (8.34 ± 1.4%), 0.5–0.71 mm (0.44 ± 0.05%), 0.71–1.0 mm (0.29 ± 0.07%), 1.0–1.7 mm (0%), >1.7 mm (0%). Experimental data indicate that the SW-FA particles are not homogeneous. According to the literature, the effectiveness of removing lead and copper ions increased with the decrease in the size of FA particles, which led to an increase in the particle surface and the number of active centers on the adsorbent having an affinity for metal ions [29,40]. Hence, literature data and research results suggested that FA with smaller particle size might be used in these studies [41–46].

The feature of SW-FA is that it is composed of particles that are characterized by various sizes, shapes and combined into agglomerations, which results in obtaining different densities. The bulk density shows the share of the total mass of particles per volume of material, and also indicates the pore volume in the mass and the volume of voids between particles. Firstly, bulk density was determined by loosely filling the cylinder with FA. In the next stage, the material was compacted on a vibrating table. The results were as follows: 0.85 ± 0.02 g/cm$^3$ and 1.51 ± 0.02 g/cm$^3$, respectively. This significant increase in the density value may be important information, for example, for companies in the case of the potential use of SW-FA as a supplement to building and construction materials.

X-ray diffraction of the sample was performed and the diffraction pattern is shown in Figure 5. Based on the analysis, it was shown that the following substances are the main crystalline phases of SW-FA: quartz (syn$SiO_2$, 48.17%), anhydrite (syn$CaSO_4$, 13.68%), sylvite (synKCl, 11.86%), calcite ($Ca(CO_3)$, 7.16%), potassium aluminum silicate ($Al_3Si_3O_{11}$, 6.73%), muscovite ($KAl_2(AlSi_3O_{10})(F,OH)_2$, 5.14%), orthoclase ($KAlSi_3O_8$, 3.66%), calcium oxide (CaO, 3.16%), periclase (synMgO, 0.43%). It should be mentioned that the sample is a combustion product and exists as a heterogeneous mixture. Hence, X-ray diffraction analysis of a sample taken elsewhere from the tank after a combustion process may reveal a different quantitative composition, but the crystalline phases of the substances should be the same. The XRD analysis was similarly noticed in the literature [35,47]. Brännvall et al. reported that fly ashes are prone to aging processes that take place when the materials are not in thermodynamic equilibrium with various conditions. The aging is influenced by

various parameters, such as redox potential, pH, temperature, humidity, the concentration of some substances in the environment, resulting in several chemical and mineralogical changes. These may be as follows: hydrolysis or hydration of K, Na, Ca, Al oxides, precipitation or dissolution of salts and hydroxides, formation, reduction and oxidation solid solutions, neoformation of clays as well as carbonation. Understanding these various transformations is essential as they can affect leaching or immobilization of hazardous substances by changes in pH, increasing or weakening mechanical stability of construction materials. In addition, aging influences the acid neutralization capacity (ANC), which is a parameter that indicates the rate of pH changes that occur when FA is affected by contact with landfill gas containing up to 50% $CO_2$ or acidic conditions (e.g., acid rain) [48].

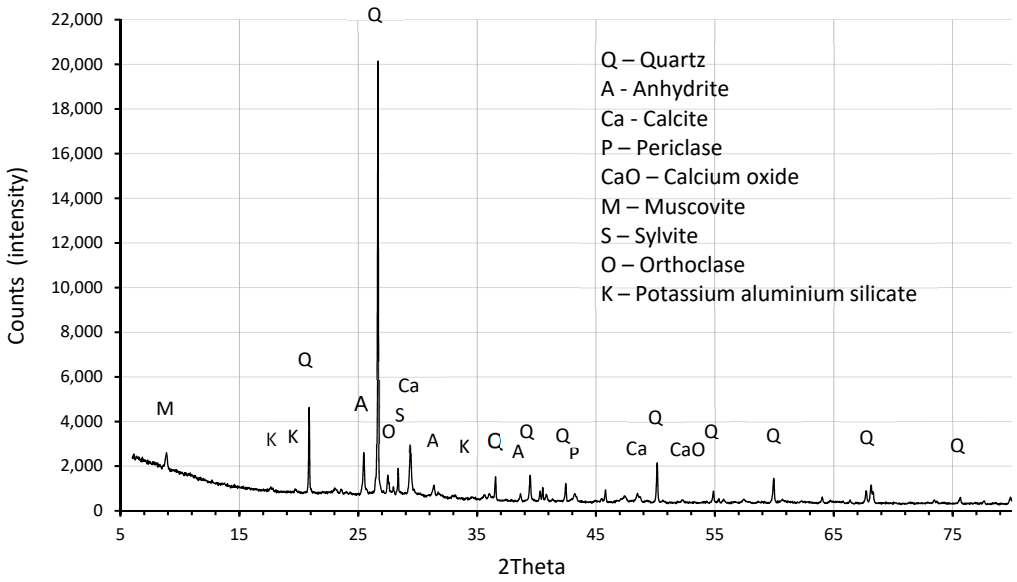


**Figure 5.** X-ray diffraction pattern of SW-FA.

Determination the elemental composition of SW-FA was carried out with X-ray fluorescence (XRF) analytical technique using an ARL Advant 'XP spectrometer (Thermo Electron Corporation, West Palm Beach, FL, USA). Based on the results presented in Table 1, it was found that $SiO_2$, $Al_2O_3$, CaO or $K_2O$ oxides have the highest share in SW-FA. It should be noted that trace amounts of CuO and PbO were observed. The results are very similar to those obtained by the XRD method.

**Table 1.** The chemical composition of SW-FA.

| Oxide | Content [%] | Oxide | Content [%] |
|---|---|---|---|
| $SiO_2$ | 50.20 | BaO | 0.06 |
| $Al_2O_3$ | 12.29 | ZnO | 0.05 |
| CaO | 11.82 | SrO | 0.046 |
| $K_2O$ | 7.99 | $ZrO_2$ | 0.025 |
| MgO | 3.34 | CuO | 0.019 |
| $P_2O_5$ | 2.04 | PbO | 0.016 |
| $Fe_2O_3$ | 1.46 | $Rb_2O$ | 0.014 |
| $Na_2O$ | 0.44 | $Cr_2O_3$ | 0.012 |
| $TiO_2$ | 0.30 | NiO | 0.006 |
| MnO | 0.28 | | |

Particle size distribution analysis was performed and the results were included as Supplementary Materials (Figure SM1). The specificity of the measurement is that SW-FA particles suspended in an aqueous solution were analyzed, and those heavier and larger in diameter got to the bottom of the suspension. Merely one peak was observed in the graph at

a particle size of 963.9 nm. According to the literature, material properties, such as strength and hydration rate are influenced by the particle size distribution [49,50]. Additionally, this parameter acts as a key indicator of particle quality and performance in many different processes. The smaller particles are able to dissolve more quickly in solution and form a more stable suspension compared to the larger ones. Moreover, smaller adsorbent particles achieve a higher efficiency in adsorption processes [41,51,52].

The SW-FA material was subjected to thermogravimetric analysis and the graph is presented in Figure 6. In general, with increasing temperature, the weight loss of the sample is observed in the temperature range from 30 to 600 °C. In the case of TG curve, denoting a change in the loss of mass, the total mass loss was about 2.53% and it was rectilinear and constant. This may be related to the get rid of adsorbed water from the SW-FA as well as carbon monoxide and volatile components, e.g., organic compounds that may have condensed on the sample. Other reaction may be associated with dehydroxylation of calcium hydroxide [45,53]. The SEM-EDS analysis indicated the presence of carbon, calcium and oxygen in the SW-FA after the combustion process. It can be assumed that oxidation of carbon to carbon dioxide took place at temperatures below 700 °C (reaction Equation (7)). As a result of the thermogravimetric analysis (TGA) there is also a further weight loss in the range 500–600 °C, which can be explained by the decomposition of $CaCO_3$ into CaO and $CO_2$ (reaction Equation (8)) [46,47,54]:

$$C + O_2 \rightarrow CO_2 \quad (7)$$

$$CaCO_3 \rightarrow CaO + CO_2 \quad (8)$$

According to our previous studies and the literature, further heating of FA at temperatures above 600 °C causes another weight loss, which may be a consequence of the deterioration of the grain wall surfaces attributable to the release of gaseous products from their internal areas [46]. DTG analysis shows the rate of weight loss as a function of temperature (derivative of weight loss [%/min]). The diagram shows three major weight losses over the temperature range of 30–70 °C (removal of free and unbound water), 300–340 °C (loss of water from hydrates (dehydration)), 550–600 °C (beginning of gaseous substances release and decomposition of carbonated products) [55]. Negative values of the DTG signals indicate the ongoing endothermic reactions. Thermal phenomena that occur in SW-FA are important from the point of view of industrial applications including heat treatment processes.

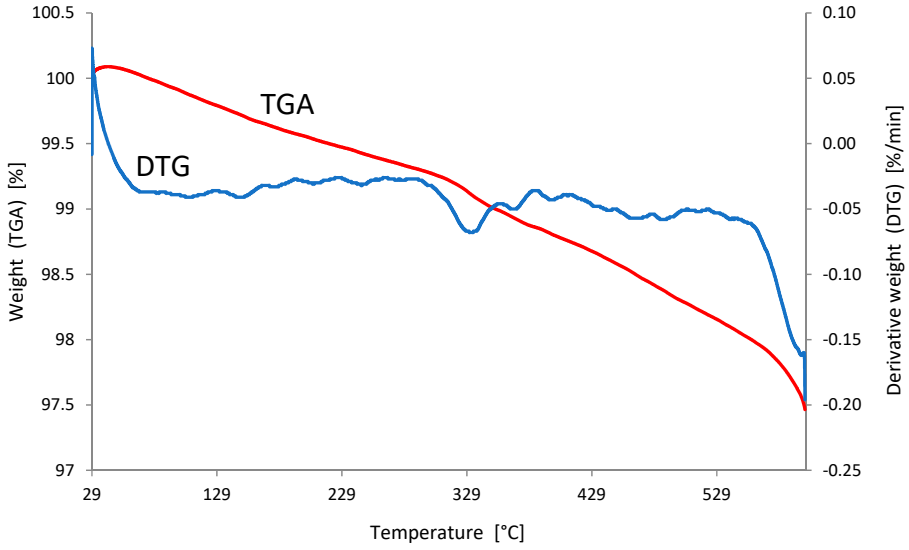


**Figure 6.** Thermogravimetric curves of SW-FA.

Electrokinetic zeta potential analysis was performed on the sample SW-FA before and after rinsing with distilled water (Figure SM2). Thanks to this parameter, it is possible to determine the impact of surface charge on the sorption of metal ions and to estimate the efficiency of this process [56]. Experimental data show that the surface charge of SW-FA varies depending on the pH of the solution and decreases from 9.79 mV (pH 2.04) to −12 mV (pH 7.15). At pH 2.0–2.6 (1.8–8.13 mV) the system is characterized by low system stability. In the range of pH 2–4, the values of surface charge indicate the prevalence of negative ions in the system. The isoelectric point (IEP) was achieved at pH 4.2, which means that the system has on average an equivalent amount of negative and positive charges. In the pH range of 4.2–7.0, positive ions are predominantly present. In the next step, the SW-FA was rinsed several times with distilled water to obtain pH 7 of the dispersion system. In this case, the curve only slightly changed, the amount of negatively charged ions decreased and the surface charge changed from 6.27 mV (pH 2.1) to −12 mV (pH 7.1). The isoelectric point (IEP) was similarly achieved at pH 4.3. At this point, SW-FA particles have the lowest osmotic pressure, viscosity, and solubility in aqueous solution.

The analysis of SEM-EDS spectrometry was performed and the results are presented in Figure SM3. The EDS spectrum shows peaks corresponding to such elements as: O, Si, C, Al, Ca, K, Ti, S, Mg, Fe, Cl, P. The SW-FA material is not homogeneous and slight quantitative differences in composition may occur at each EDS measuring point on the material surface. Additionally, the SEM-EDS mapping method using a backscattered detector was used to determine the distribution of various elements on the material. The images show different distribution of individual elements, and their intensity is dependent on the type of element, but also on the combustion process or properties and chemical composition of sunflower and wood waste (Figure SM4). The multi-component composition of FA affects its favorable physicochemical properties, hence it can be used in industry as an additive to building and construction materials (concrete, bricks), ceramics, soil treatment, zeolite synthesis, but also as a material useful for removing pollutants from air and water due to its good binding properties. FA from biomass combustion can be used as an additive to fertilizers, but also to fertilize soils, especially in forests. On the other hand, FA from the combustion of coal and a mixture of wood and biomass waste is currently used for the foundation of roads, filling post-mining voids [57–59].

BET analysis was performed to analyze porosity of SW-FA (Figures SM5–SM21) and determined parameters, such as specific surface area ($S_{BET}$), pore volume ($V_p$) and average pore diameter ($Apd$) are presented in Table 2. The analysis showed that the shape of the isotherms resembled type III isotherms, being convex towards the pressure axis. In addition, the shape informs about the so-called cooperative adsorption, meaning that previously adsorbed molecules allow for an increase in the adsorption of residual particles present in the solution. If the particles have already been adsorbed on the adsorbent, the adsorbate—adsorbate interaction has a positive effect on the adsorption of other ions, which results in the enhancement of the isotherm towards the pressure axis. The type III isotherm indicates that the adsorbed molecules are clustered around the most favorable places on the surface of a nonporous or macroporous adsorbent [60].

The adsorptive and desorptive pore volume distribution was analyzed by the use of the BJH method, the principle of which is that nitrogen gas is adsorbed on a specific surface and is in relation to the relative pressure of the adsorbent. While the temperature is constant, the adsorption isotherm is associated with the connection between gas adsorption and gas balance relative pressure. Based on the desorption line of isothermal adsorption curve, the calculation of pore size distribution is carried out by determining the amount of nitrogen adsorbed at a relative pressure of 0.99 using Equation (9):

$$V_{pn} = \left(\frac{r_{pn}}{r_{kn} + \Delta t_n}\right)^2 \left(\Delta V_n - \Delta t_n \sum_{j-1}^{n-1} A_{cj}\right) \quad (9)$$

where: $V_{pn}$—the pore volume; $t_n$—the adsorbed nitrogen layer thickness; $r_{kn}$—the capillary radius; $r_{pn}$—the maximum pore radius; $A_{cj}$—the area after the emptying; $V_n$—capillary volume [61].

The BJH method is related to capillary condensation appearing in the pores. During the capillary condensation process, pressure increase causes an increase in the thickness of the adsorbate layer on the pore walls [62]. In this way, the adsorption isotherms were determined and the volume and distribution based on the size of the pores were obtained (Table 2). The form of the isotherm indicates that the SW-FA probably has a non-porous structure and that slit pores are formed between the gaps of FA particles, some of which are meso-sized. The results as graphs are presented in the figures attached as Supplementary Materials.

**Table 2.** Adsorption and desorption surface parameters of SW-FA.

| Parameters | Values |
|---|---|
| BET adsorption cumulative surface area ($S_{BET}$) [$m^2/g$] | 3.264 |
| BET desorption cumulative surface area ($S_{BET}$) [$m^2/g$] | 3.660 |
| BJH adsorption cumulative volume of pores (Vpa) [$cm^3/g$] | 0.014325 |
| BJH desorption cumulative volume of pores (Vpd) [$cm^3/g$] | 0.014752 |
| BJH adsorption average pore diameter (Apda) [nm] | 17.553 |
| BJH desorption average pore diameter (Apdd) [nm] | 16.1218 |

The surface morphology of the SW-FA particles was analyzed with a scanning electron microscope (SEM) and the images are shown in Figure 7. Generally speaking, the particles have irregular shapes of various sizes. Shape irregularities appear with both larger and smaller particles. Characteristic are heterogeneous structure, porous surface, sharp ends and visible developed flat surfaces. The particles are combined into agglomerates of polygonal, shorter, longer or oval lumps, often resembling various sharp-edged crystals. Spherical shapes with microscopic structure were not observed. The particles take an irregular, elongated or acicular shape depending on the parameters of the combustion process, such as temperature and time. Spherical or crystalline shapes are formed during a longer combustion process. Similar observations were observed in the literature [35,63,64]. Gao et al. reported that the surface morphology and specific surface area of FA particles influence the surface energy of particles, which is the force initiating the processes at the liquid-sorbent interphases. FA particles have a stronger surface activity and a higher surface energy for a finer specific surface area. Additionally, FA porosity depends on the extent of the particle distribution, grain shape and microporosity [65]. Based on granulation analysis, the most particles are contained in the fraction with the grain size range 0–212 µm and particle size distribution analysis indicated SW-FA particle size of 963.9 nm. BET adsorption specific surface area is 3.264 $m^2/g$. Hence, it should be stated that the larger the specific surface area and the finer particle size distribution of the FA adsorbent, as well as the greater its adsorption capacity and interaction with metal ions [66].

### *3.2. Adsorption Studies of Pb(II) and Cu(II) Ions*

#### 3.2.1. Analysis of pH Profile

In the next stage of the research, the influence of initial and equilibrium pH on the adsorption process was analyzed. Increasing the ionization of functional groups on the adsorbent surface occurs at lower pH values, which in turn is favorable for the adsorption process. In alkaline solutions with higher pH values, Pb(II) and Cu(II) metals have ability to precipitate in the form of hydroxides [67,68]. Therefore, based on the literature and our experience from previous studies, the following experimental conditions were used: the initial concentration of metal ions 100.1–100.2 mg/L, SW-FA dosage 2–5 g/L, pH range of 1.5–2.7, contact time 60 min, rotation speed 200 rpm, T = 23 ± 1 °C. After analyzing the results presented in Figure 8 and Figure SM24, it was found that pH significantly influences the efficiency of the process. In all cases of SW-FA doses (2–5 g/L), an increase

in adsorption from the minimum to the highest values was demonstrated. The maximum adsorption efficiency was achieved in the following cases: A) Pb(II): 99.76% (initial pH 2.06, equilibrium pH 7.07, 2 g/L SW-FA), 99.81% (in. pH 2.64, eq. pH 7.59, 3 g/L SW-FA), 97.80% (in. pH 1.87, eq. pH 6.96, 4 g/L SW-FA), 99.56% (in. pH 2.05, eq. pH 6.86, 5 g/L SW-FA); B) Cu(II): 99.15% (in. pH 2.08, eq. pH 7.11, 2 g/L SW-FA), 99.53% (in. pH 2.68, eq. pH 7.6, 3 g/L SW-FA), 98.20% (in. pH 1.94, eq. pH 6.97, 4 g/L SW-FA), 99.61% (in. pH 2.15, eq. pH 6.86, 5 g/L SW-FA). The results show that the initial pH affects the adsorption efficiency and capacity relative to different doses of SW-FA. Probably the cation exchange mechanism was responsible for binding these metal ions. In aqueous solutions, the SW-FA surface and functional groups could be protonated by available hydrogen ions, which increased the number of positively charged active centers and decreased the number of negative ones. In water, competition takes place between $Pb^{2+}$, $Cu^{2+}$ ions and $H^+$ ions, which are not beneficial for metal adsorption due to electrostatic repulsion. The gradual increase in the pH value caused negative electrostatic charging of the SW-FA surface and deprotonation of groups containing $H^+$ ions. This situation favored greater adsorption of metal ions. According to the literature, lead and copper exist in the ionic form in pH range 2–7 and 2–6.5, respectively. On the other hand, at higher pH, these metals precipitate in the form of $Pb(OH)_2$ and $Cu(OH)_2$ hydroxides [69–71]. Hence, the maximum adsorption was obtained at lower pH. Additionally, the literature describes the process of Pb(II) and Cu(II) adsorption, taking into account the influence of many factors (including pH) [72–74]. The XRD analysis showed the presence of $SO_4^{2-}$, $Cl^-$, $CO_3^{2-}$, $OH^-$, $SiO_3^{2-}$ anions which means that they could participate in the precipitation of Cu(II) and Pb(II) ions. Based on the XRF analysis, many metal oxides are present in the sample. Their electrostatic charge and behavior are strongly influenced by pH of aqueous solution. Hence, with a high degree of probability the complexation through ion exchange could take place. The complexation process of $Pb^{2+}$ and $Cu^{2+}$ ions with oxygen groups was accompanied by the release of $H^+$ cations. The mechanism can be generally presented according to Equations (10)–(13):

$$-XOH + H_3O^+ \rightarrow XOH_2^+ + H_2O \quad (10)$$

$$-XOH + OH^- \rightarrow XO^- + H_2O \quad (11)$$

$$2(-XO^-) + Pb^{2+} \rightarrow (-XO)_2Pb \quad (12)$$

$$2(-XO^-) + Cu^{2+} \rightarrow (-XO)_2Cu \quad (13)$$

where: X can be Si, Al, Ca, K or other. As the pH of the solution increased, the number of anions, dissociated from hydroxyl groups on the surface of SW-FA, also increased, with a consequence of increasing electrostatic attraction capacity between the interacting ions. Nevertheless, these possible mechanisms have not been confirmed with appropriate experiments in these studies [45,75].

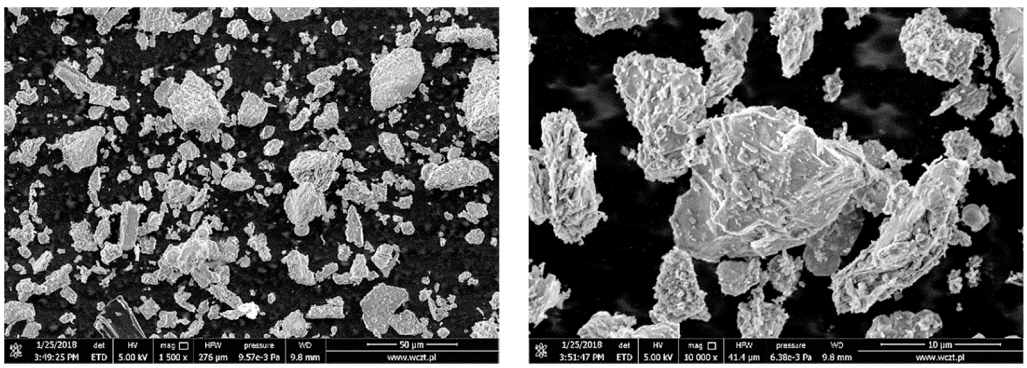

(**a**) (**b**)

**Figure 7.** SEM images of SW-FA: (**a**) magn. 1500×, scale bar: 50 μm, (**b**) 10,000×, 10 μm.

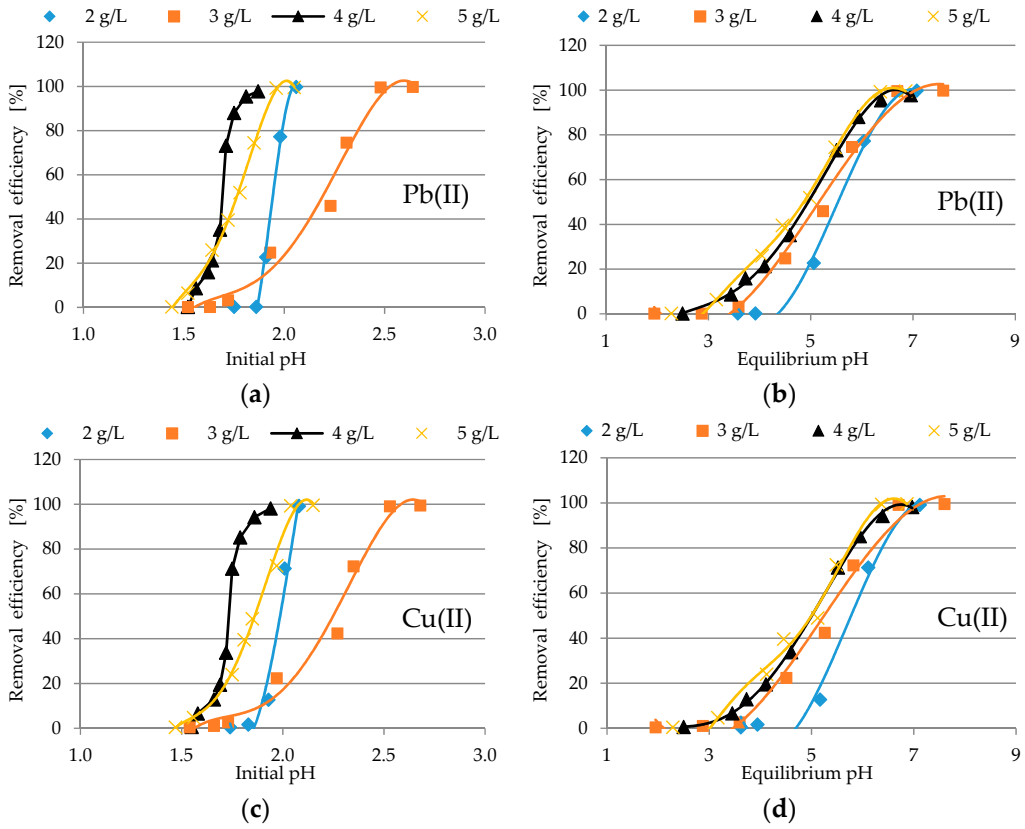


**Figure 8.** The dependence between initial (**a**,**c**) and equilibrium pH (**b**,**d**) and removal efficiency of Pb(II) and Cu(II) ions with SW-FA.

### 3.2.2. Impact of Adsorbent Dosage

The influence of SW-FA dosage on the efficiency of Pb(II) and Cu(II) removal from aqueous solutions was investigated and the results are presented in Figure 9a,b. The following experimental conditions were used: initial concentration of metal ions 20–100 mg/L, initial pH 2.2, rotational speed 200 rpm, T = 23 ± 1 °C, contact time 60 min. As it is seen in these experimental conditions, the adsorbent dose of 3 g/L can be considered optimal due to the highest efficiency at the tested pH and the initial concentration range of 20–100 mg/L. Further increase of the SW-FA dosage was not necessary as no significant changes in the adsorption process were observed. The maximum sorption results for the SW-FA dosage of 5 g/L are as follows: A) Pb(II): 98.85% (20 mg/L Pb(II)), 99.48% (40 mg/L), 99.67% (60 mg/L), 99.76% (80 mg/L), 99.81% (100 mg/L); Cu(II): 98.16% (20 mg/L Cu(II)), 99.08% (40 mg/L), 99.30% (60 mg/L), 99.55% (80 mg/L), 99.64% (100 mg/L). In addition, an initial increase in calculated adsorption capacity was observed at 1 to 3 g/L SW-FA dosages, followed by a decrease at higher values of 4 and 5 g/L (Figure SM22). The increase depends on the initial concentration of the metals. The highest values of the adsorption capacity were reported at the dose of 2–3 g/L and are as follows: A) Pb(II): 9.76 mg/g (20 mg/L Pb(II)), 15.44 mg/g (40 mg/L), 19.92 mg/g (60 mg/L), 26.55 mg/g (80 mg/L), 32.94 mg/g (100 mg/L); B) Cu(II): 9.11 mg/g (20 mg/L Cu(II)), 14.77 mg/g (40 mg/L), 19.80 mg/g (60 mg/L), 26.48 mg/g (80 mg/L), 32.70 mg/g (100 mg/L). In this process, at lower doses of SW-FA, the active sites could be fully occupied by metal ions when interacting with the adsorbent, and at higher doses, they could not be fully utilized. The decrease in adsorption capacity is related to an increase in the SW-FA dose and thus an increase in the number of available sites capable of binding metal ions. Similar results of studies involving FA are confirmed in the literature [45,46,76,77]. Harja et al. also reported in their studies on Cu(II) adsorption with FA and FA/$Fe_3O_4$ that 'adsorption capacity decreases with an increase in the adsorbent dose' due to 'the aggregation of the magnetic particles' [78]. Militaru et al.

revealed that as sewage sludge ash dose increases, the adsorption efficiency of Pb(II) and Cu(II) increases as well, and it was higher in the case of Pb(II), quite similar to results in this research studies [79].

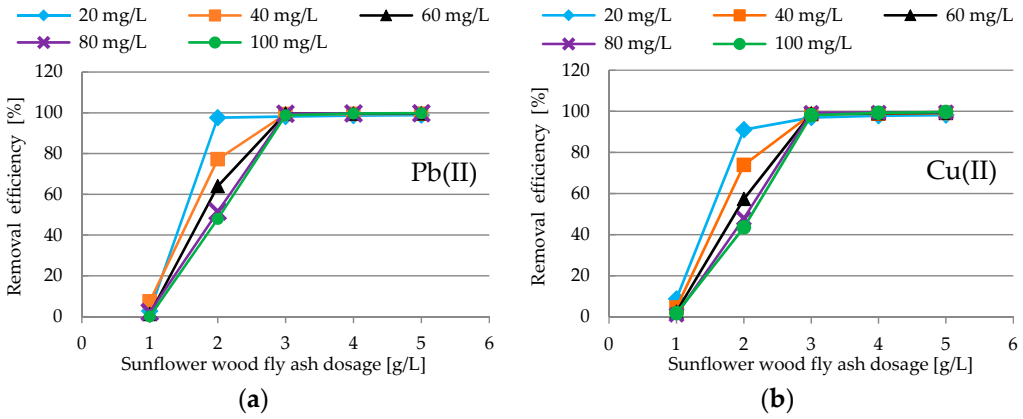


**Figure 9.** The impact of SW-FA dosage on adsorption efficiency of Pb(II) (**a**) and Cu(II) (**b**) ions.

### 3.2.3. Impact of Initial Concentration of Pb(II) and Cu(II)

The adsorption properties at different initial concentrations of Pb(II) and Cu(II) ions were investigated, and the results are presented in Figure 10. The analysis of the previously conducted tests allowed for the use of the following experimental conditions in this stage: initial concentration of metal ions 20–100 mg/L, doses of adsorbent 1–5 g/L, initial pH 2.2, contact time 60 min, rotational speed 200 rpm, T = 23 ± 1 °C. As observed, the lowest adsorption occurs at a lower dose of 1 g/L. As observed, the lowest adsorption occurs at a lower dose of 1 g/L. At the dose of 2 g/L, the adsorption increased to about 60%. However, at higher doses of 3–5 g/L, the maximum adsorption efficiency was equal to 99.76% (Pb(II)) and 99.49% (Cu(II)). The equilibrium pH after the entire sorption process ranged from 3.5 to 8.3. Moreover, a constant increase in the adsorption capacity was observed in the range from the minimum values (0.32–2.3 mg/g for Pb(II), 0.91–2.44 mg/g for Cu(II)) to the maximum value of 33.47 mg/g for Pb(II) and 33.3 mg/g Cu(II) (Figure SM23).

The analysis of the sorption process showed that the initial concentration of metal ions has an influence on the saturation of the SW-FA surface. However, at higher concentrations, the process of intramolecular diffusion of metal ions on the SW-FA surface could take place. In aqueous solutions with low acidic pH, the hydrous oxide (MOH) surface of the adsorbent will be fully covered by $H^+$ ions ($MOH + H^+ \rightarrow MOH_2^+$). As a result, the greater positive electrostatic charge appears on the surface of the adsorbent and the adsorption of metal ions becomes more complex. Competition between $H^+$ ions and Cu(II) or Pb(II) ions for the active surface centers and lower adsorption was noted. In alkaline solutions, negative charge is dominant and hydroxide ions can react with hydrous oxides to form deprotonated particles ($MOH + OH^- \rightarrow MO^- + H_2O$). The adsorbent surface becomes deprotonated, which results in electrostatic attraction between the positively charged metal ions and the negatively charged adsorbent surface [77,80]. Figure 10 shows that the initial low metal concentration of 20 mg/L has already caused the first ion exchange reactions at the interface between the aqueous and solid phase. According to the literature, $Pb^{2+}$ and $Cu^{2+}$ ions have ionic radii of 0.119 Å and 0.73 Å, respectively. If ionic radius of metal ions is smaller, the easier it is to hydrolyze in aqueous solutions. Furthermore, hydrolysed molecules have lower ability to adsorb on the adsorbent surface, which is related to the lower efficiency of the adsorption process [79–83].

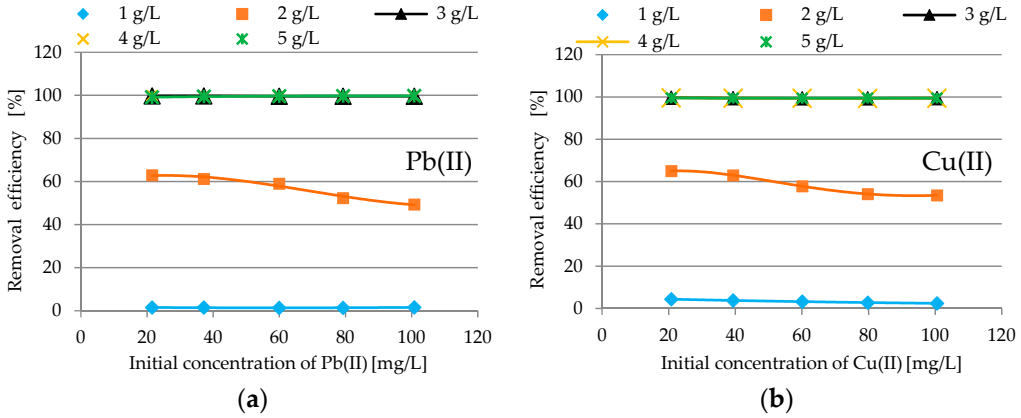


**Figure 10.** The impact of initial concentration of Pb(II) (**a**) and Cu(II) (**b**) ions on SW-FA removal efficiency.

### 3.2.4. Reaction Kinetics

#### Contact Time Studies

The contact time parameter is important for industrial applications, hence its influence on adsorption was investigated and the results are shown in Figure 11 and Figure SM25. Determining the optimal contact time in the process is important when properly designing the entire adsorption process, as well as reducing costs and energy consumption. Based on our previous research, the following experimental conditions were proposed: initial concentration 100.2 mg/L, initial pH 2.0, SW-FA dosage 5 g/L, contact time range 0–60 min, rotation speed 200 rpm, T = 23 ± 1 °C. The obtained results indicated that the best adsorption efficiency was reported within the first 5 min of the process and there were no significant changes up to 60 min. Hence, it was not necessary to conduct research on longer time of adsorption. The results after 5 min. were as follows: 99.01%, 19.84 mg/g, equilibrium pH 5.04 (Pb(II)) and 98.76%, 19.79 mg/g, equilibrium pH 4.75 (Cu(II)). The rapid initial increase in adsorption is the hallmark of the SW-FA material. This phenomenon can have many reasons, such as: high concentration of metal ions at the water-solid interface, high electrostatic attraction on the adsorbent surface, and the availability of a larger number of free active sites on the SW-FA surface. The mechanism of ion exchange reactions can take various forms, but after each of them, the equilibrium of the entire process is gradually achieved through the occupation of active centers by metal cations [10,84]. Likewise, Hałas et al. reported in their studies of contact time that during the first stage, rapid and intensive sorption of Cu(II), Fe(III), Mn(II) and Zn(II) was observed because of large availability of surface active sites. The second step was much slower, because the process remained at the same level and reached equilibrium as most of the active sites were adsorbed. Other processes could also take place, such as ion exchange, interactions between metal ions and functional groups of the adsorbent, and diffusion of metals into its structure [85]. Alinnor reported in his study that at higher pH, the FA surface was negative and the adsorption of Cu(II) and Pb(II) ions increased. This could be caused by electrostatic interaction, which was manifested by a sudden increase in the amount of adsorbed metal ions when the pH value increased from the initial 6 to the equilibrium value of 10. This can be attributed to the contents of $SiO_2$, $Fe_2O_3$, $Al_2O_3$ and Ca in FA, which increase pH to strongly alkaline values and increase the adsorption of Cu(II) and Pb(II) ions. The simultaneous precipitation and adsorption of the metal ions on FA surface can also occur at low pH values ranging from 4 to 6. Hydration of FA increases pH to values in the range 10–13 and is a consequence of a developed precipitation degree of metal ions, and to increase their adsorption [86].

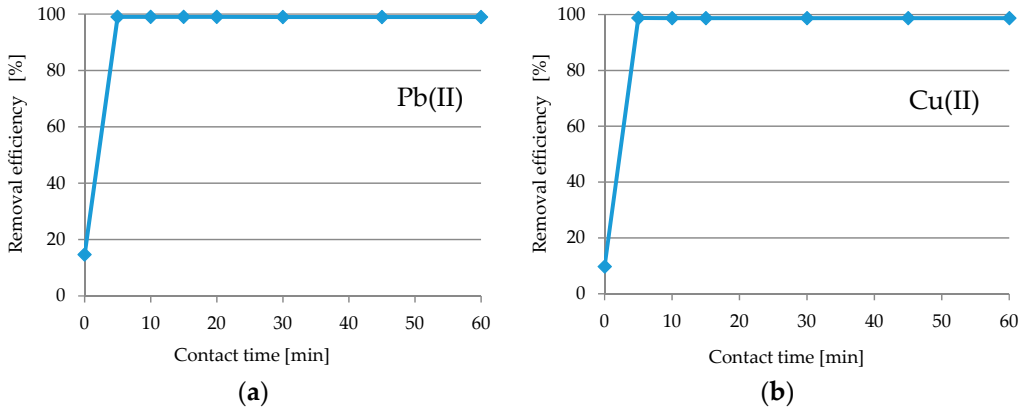


**Figure 11.** The impact of contact time on the Pb(II) (**a**) and Cu(II) (**b**) ions removal efficiency.

Pseudo-First-Order and Pseudo-Second-Order Kinetic Models

The kinetics of the adsorption of Pb(II) and Cu(II) ions was analyzed. For this purpose, a pseudo-first-order and pseudo-second order model was applied. The kinetic parameters of these models were determined and the results are presented in Table 3 and Figures SM26–SM29. Higher correlation coefficients $R^2$ (0.999 and 0.999) were obtained for the pseudo-second reaction model, which better fits the description of kinetics of the adsorption process. Pb(II) and Cu(II) ions could be bound by the process of chemical reaction, create chemical bonds and have an affinity for active sites, which resulted in high adhesion to the SW-FA surface [87]. Under the conditions of a lower concentration of metal ions in aqueous solutions, the particles collided with each other less frequently. The situation of lower intensity of obstacles in the solution meant that metal ions could bind to SW-FA active centers much faster.

**Table 3.** Adsorption parameters of pseudo-first-order and the pseudo-second-order rate equations.

| Metal Ion | Adsorbent Dosage [g/L] | Pseudo-First-Order Kinetic Model | | | Pseudo-Second-Order Kinetic Model | | |
|---|---|---|---|---|---|---|---|
| | | $k_{ad}$ [min$^{-1}$] | $q_e$ [mg/g] | $R^2$ | $k$ [g/mg min] | $q_e$ [mg/g] | $R^2$ |
| **Pb(II)** | 5 | 0.086 | 0.052 | 0.828 | 106.14 | 0.212 | 0.999 |
| **Cu(II)** | 5 | 0.124 | 0.046 | 0.878 | 72.66 | 0.257 | 0.999 |

3.2.5. Isothermal Studies

In these studies, Langmuir and Freundlich isothermal models were used to further describe the adsorption process (Figures SM30–SM33). The calculated parameters of the isotherms indicate that the process fits the Freundlich model better (Table 4). The Freundlich isotherm relates to the relationship between the concentration of metal ions in a liquid at equilibrium (*Ce*) and the concentration of dissolved ions on the surface of the adsorbent (*qe*). The determined values of the Freundlich isotherm parameters ($K_f$—adsorbent adsorption capacity index, $n$—adsorption intensity index) suggest that Pb(II) and Cu(II) ions can easily separate from the solution. In these studies, the highest calculated adsorption capacity (Langmuir parameters) was as follows: 138.37 mg/g (Pb(II), 5 g/L SW-FA) and 97.43 mg/g (Cu(II), 5 g/L SW-FA).

**Table 4.** Isotherm model constants and correlation coefficients for adsorption of Pb(II) and Cu(II) using SW-FA.

| Metal Ion | Adsorbent Dosage [g/L] | Langmuir Isotherm | | | Freundlich Isotherm | | |
|---|---|---|---|---|---|---|---|
| | | Calculated $q_m$ [mg/g] | $K_L$ [L/mg] | $R^2$ | $K_f$ [mg/g] [L/mg]$^{(1/n)}$ | $n$ | $R^2$ |
| **Pb(II)** | 1 | 16.18 | 0.0009 | 0.998 | 0.019 | 1.080 | 0.999 |
| | 2 | 46.37 | 0.024 | 0.956 | 2.145 | 1.584 | 0.990 |
| | 3 | 68.76 | 2.228 | 0.966 | 57.344 | 1.430 | 0.989 |
| | 4 | 72.92 | 1.325 | 0.963 | 57.504 | 1.167 | 0.967 |
| | 5 | 138.37 | 0.537 | 0.992 | 61.209 | 1.045 | 0.996 |
| **Cu(II)** | 1 | 7.57 | 0.007 | 0.953 | 0.148 | 1.608 | 0.984 |
| | 2 | 48.53 | 0.02 | 0.981 | 1.686 | 1.390 | 0.993 |
| | 3 | 65.63 | 1.597 | 0.957 | 46.24 | 1.357 | 0.982 |
| | 4 | 72.63 | 0.818 | 0.979 | 35.48 | 1.223 | 0.989 |
| | 5 | 97.43 | 0.462 | 0.989 | 34.08 | 1.102 | 0.990 |

### *3.3. FT-IR Analysis*

FT-IR analysis of SW-FA was carried out before and after the adsorption process, and the corresponding spectra are presented in Figure 12. The following experimental conditions were used in this study: SW-FA dose 5 g/L, initial concentration of Pb(II) and Cu(II) ions 10 mg/L, initial pH 2.0, T = 23 ± 1°C, contact time 60 min. The explanation of FT-IR peaks and their wavelengths are explained in Table 5. The spectra were interpreted before and after the adsorption process, taking into account the intensity of bands, frequency, shape differences and possible interactions of functional groups with Pb(II) and Cu(II) ions. As it is seen in Figure 12, after the adsorption process, the intensity of the bands changed towards other transmittance values. The positions of the bands were either at the same wavelengths or slightly shifted. These changes are as follows: 3261.76 (shift to 3258.62 $cm^{-1}$ (Pb(II)) and 3314.28 $cm^{-1}$ (Cu(II))), 1412.41 (shift to 1410.22 $cm^{-1}$ (Pb(II)) and 1414.53 $cm^{-1}$ (Cu(II))), 985.11 (shift to 984.74 $cm^{-1}$ (Pb(II)) and 984.27 $cm^{-1}$ (Cu(II))), 874.03 (shift to 874.28 $cm^{-1}$ (Pb(II)), 678.61 (shift to 712.96 $cm^{-1}$ (Pb(II)) and 693.48 $cm^{-1}$ (Cu(II))), 430.92 (shift to 422.84 $cm^{-1}$ (Pb(II)) and 432.25 $cm^{-1}$ (Cu(II))). The peak shifts are a consequence of the interaction and binding of metal ions with functional groups present on the SW-FA surface and confirmed by the XRF analysis. Comparing these results with literature, for example FA from the combustion of wood chips and deciduous trees waste was used for FT-IR research. There was reported similar bands related to the following vibrations: asymmetric stretching Si-O (1110 $cm^{-1}$, 1044 $cm^{-1}$), symmetric stretching Si-O-Si (796 $cm^{-1}$), symmetric stretching Al-Si-O (571 $cm^{-1}$), bending O-Si-O (467 $cm^{-1}$, silica glass and quartz) [88].

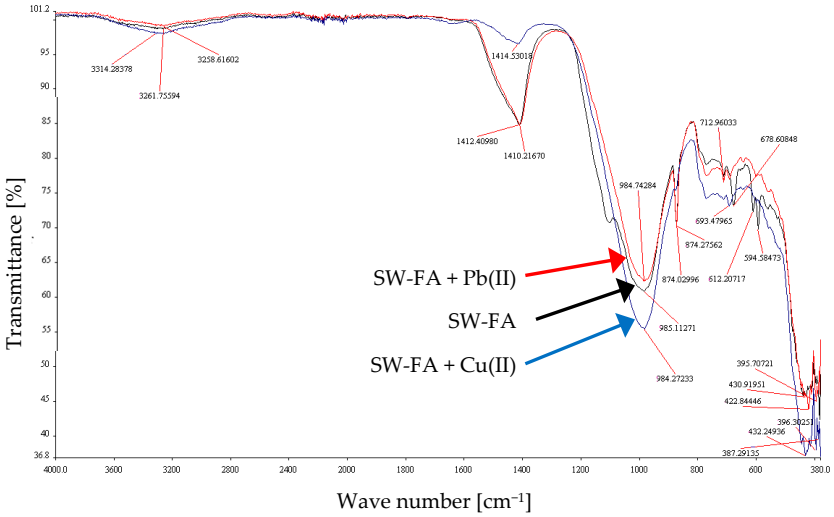


**Figure 12.** FT-IR spectrum of SW-FA before and after Pb(II) and Cu(II) ions adsorption.

**Table 5.** FT-IR peaks of SW-FA and explanation.

| FT-IR Band [cm$^{-1}$] | Assignment (Vibrations, Species) |
|---|---|
| 3258.6, 3261.8, 3314.28 | stretching vibrations O–H |
| 1410.2, 1412.4, 1414.53 | valence vibration of carbonate ions |
| 984.7, 984.27, 985.1 | asymmetric stretching vibrations of silica Si–O–Si and Al–O–Si |
| 873.3, 874.03, 874.28 | symmetric stretching of Al–O–M, vibration of carbonates (calcite) |
| 713 | symmetric stretching of Si–O–Si and Al–O–Si |
| 678.6, 693.5, 678.6 | stretching vibrations Al–O |
| 612.2 | stretching vibrations Al–O |
| 594.6 | vibrations Si-O-Pb |
| 396.3, 395.7, 387.3, 422.8, 430.9, 432.2 | bond bending vibrations Si-O-Si |

## 4. Conclusions

In this study, fly ash produced as a result of the incineration of sunflower (20%, *m/m*) and wood (80%, *m/m*) waste (SW-FA) using the circulating fluidized bed combustion (CFBC) technology was examined for the possibility of adsorption of Pb(II) and Cu(II) ions from aqueous solutions. The physicochemical and textural properties of SW-FA have been evaluated using a number of research methods to provide the most complete characterization of the material. The granulation analysis showed the most SW-FA particles in the diameter range of 0–212 µm (90.93%), while the particle size distribution analysis showed mainly the size of 963.9 nm. The bulk density was equal to 0.85 g/cm$^3$ (loosely filling the cylinder) and 1.51 g/cm$^3$ (compacted on a vibrating table). Based on the XRD analysis, the following substances were identified: quartz, anhydrite, sylvite, calcite, potassium aluminum silicate, muscovite, orthoclase, calcium oxide and periclase. The XRF analysis showed the content of mainly oxides such as: $SiO_2$ (50.2%), $Al_2O_3$ (12.3%), CaO (11.8%), $K_2O$ (8%), MgO (3.3%), $P_2O_5$ (2%), $Fe_2O_3$ (1,5%). Thermogravimetric analysis (TGA) presented that with increasing temperature, the weight loss was observed in the temperature range from 30 to 600 °C (in total approx. 2.53%). Electrokinetic zeta potential analysis showed the predominance of negative ions at pH 2–4 and positive ones at pH 4.2–7.0. The isoelectric point (IEP) was reached at pH 4.2. According to the EDS analysis, the following elements were determined: O, Si, C, Al, Ca, K, Ti, S, Mg, Fe, Cl, P. The SEM-EDS mapping method revealed different distribution of individual elements and their intensity. The BET and BJH analysis determined adsorption parameters, such as specific surface area (3.264 m$^2$/g), pore volume (0.014325 cm$^3$/g) and average pore diameter (17.553 nm). The shape of the isotherms resembled type III isotherms, being convex towards the pressure

axis, which informed about the so-called cooperative adsorption. The adsorbent consists of slit pores formed between particles, some of which are meso-sized. The analysis of SEM surface morphology revealed that the SW-FA particles are combined into agglomerates, have irregular shapes of various sizes, porous surface, sharp ends and visible developed flat surfaces.

The effectiveness of the adsorption process was established on the basis of the analysis of the effect of sorbent dose, initial and equilibrium pH, initial concentration and contact time. The obtained research results gave a clear message that in many experimental conditions the efficiency of the process was high and ranged from 90 to 100%. The maximum removal efficiency for Pb(II) was 99.81% (initial pH 2.64, equilibrium pH 7.59, initial concentration 100.1 mg/L, SW-FA dosage 3 g/L) and for Cu(II) was 99.61% (initial pH 2.15, equilibrium pH 6.86, initial concentration 100.1 mg/L, SW-FA dosage 5 g/L) at contact time 60 min, rotational speed 200 rpm, T = 23 ± 1 °C. The binding of metal ions by functional groups was confirmed not only by AAS measurements, but also by changes in the intensity of bands and slight shifts of peaks visible in the FT-IR spectrum. The process was described by the analysis of kinetics and determination of isotherms. It has been shown that the kinetic model of pseudo-second-order reaction and Freundlich model best describe the adsorption processes. Based on the Langmuir equation, the calculated maximum adsorption capacity $q_{max}$ is 138.37 mg/g for Pb(II) (5 g/L SW-FA) and 97.43 mg/g for Cu(II) (5 g/L SW-FA).

In summary, it can be stated that the fly ash formed as a result of combustion of post-production sunflower and wood waste is capable of removing Pb(II) and Cu(II) ions with a very high process efficiency due to the content of appropriate functional groups and favorable properties of the adsorbent. The results of the experiments gave sufficient reasons to continue research on the use of SW-FA in the processes of adsorptive removal of other metal ions. Currently, great emphasis is placed on improving water quality through its purification using various methods. Certainly, the use of SW-FA waste in cheap adsorption processes can be successfully used in industry for the removal various metal ions from waste waters, including Cu, Pb, Zn, Mn, Cd, Cr, Ni, Fe, Al, Ti, Ge, Ga, U, Li, precious metals and others (e.g., phenol derivatives, flue gas desulphurisation). After adsorption processes, the SW-FA samples could be disposed of safely by solidification, vitrification or burning after drying. The beneficial properties of SW-FA allow for other industrial applications, including the use as a soil amelioration agent for agricultural purposes; as porous material for separation and catalytic processes due to its potential to reduce the consumption of materials that have limited reserves and/or are expensive to produce; as a low cost material for the production of ceramics, glass-ceramics, and glass materials due to the content of $SiO_2$, $Al_2O_3$, CaO, and $Fe_2O_3$; as a component in the synthesis of geopolymers that can be used in construction, transport, aerospace, mining, and metallurgy industry. All these applications make them fit into the latest global trends in circular economy, they can contribute to the reduction of $CO_2$ emissions, so the impact on climate neutrality.

**Supplementary Materials:** The following are available online at https://www.mdpi.com/1996-1073/14/6/1771/s1, Figure SM1: Particle size distribution of SW-FA determined by laser diffraction, Figure SM2: Electrokinetic zeta potential of SW-FA before and after rinsing with distilled water, Figure SM3: EDS spectrum of SW-FA, Figure SM4: SEM–EDS images (mapping) of the distribution and relative proportion (intensity) of defined elements (C, O, Mg, Al, Si, P, S, Cl, K, Ca, Ti, Fe) over the scanned area of SW-FA (scale bar: 20 µm), Figure SM5: The low temperature BET adsorption and desorption isotherm linear plot, Figure SM6: BET surface area plot, Figure SM7: Langmuir surface area plot, Figure SM8: Harkins and Jura t-plot, Figure SM9: BJH adsorption cumulative pore volume, Figure SM10: BJH adsorption dV/dD pore volume, Figure SM11: BJH adsorption dV/dlog(D) pore volume, Figure SM12: BJH adsorption cumulative pore area, Figure SM13: BJH adsorption dA/dD pore area, Figure SM14: BJH adsorption dA/dlog(D) pore area, Figure SM15: BJH desorption cumulative pore volume, Figure SM16: BJH desorption dV/dD pore volume, Figure SM17: BJH desorption dV/dlog(D) pore volume, Figure SM18: BJH desorption cumulative pore area, Figure SM19: BJH desorption cumulative pore area, Figure SM20: BJH desorption dA/dD pore area,

Figure SM21: BJH desorption dA/dlog(D) pore area, Figure SM22: The impact of SW-FA dosage on adsorption capacity of Pb(II) and Cu(II) ions, Figure SM23: The impact of initial concentration of Pb(II) and Cu(II) ions on SW-FA adsorption capacity, Figure SM24: The dependence between initial and equilibrium pH and Pb(II) and Cu(II) adsorption capacity of SW-FA, Figure SM25: The impact of contact time on adsorption capacity of SW-FA during the removal of Pb(II) and Cu(II) ions, Figure SM26: Pseudo-first-order isotherm for adsorption of Pb(II) ions with SW-FA, Figure SM27: Pseudo-first-order isotherm for adsorption of Cu(II) ions with SW-FA, Figure SM28: Pseudo-second-order isotherm for adsorption of Pb(II) ions with SW-FA, Figure SM29: Pseudo-second-order isotherm for adsorption of Cu(II) ions with SW-FA, Figure SM30: Langmuir isotherms for adsorption of Pb(II) ions with SW-FA, Figure SM31: Langmuir isotherms for adsorption of Cu(II) ions with SW-FA, Figure SM32: Freundlich isotherms for adsorption of Pb(II) ions with SW-FA, Figure SM33: Freundlich isotherms for adsorption of Cu(II) ions with SW-FA.

**Author Contributions:** Conceptualization, T.K. and R.C.; methodology, T.K. and R.C.; validation, T.K., R.C. and M.U.; formal analysis, T.K.; investigation, T.K. and R.C.; resources, T.K., R.C. and M.U.; data curation, T.K. and R.C.; writing—original draft preparation, T.K.; writing—review & editing, T.K.; visualization, T.K.; supervision, T.K. and R.C.; project administration, T.K. and R.C.; funding acquisition, T.K., R.C. and M.U. All authors have read and agreed to the published version of the manuscript.

**Funding:** This research did not receive a specific grant from any a funding agency in the public, commercial or not-for-profit sectors.

**Institutional Review Board Statement:** Not applicable.

**Informed Consent Statement:** Not applicable.

**Data Availability Statement:** Data is contained within the article.

**Conflicts of Interest:** The authors declare no conflict of interest.

## References

1. Kalak, T. *Responsibility for Marine Litter Floating in the North Pacific Ocean*; LAP Lambert Academic Publishing: Sunnyvale, CA, USA, 2018; ISBN 978-613-9-94366-1.
2. Ramana, D.K.V.; Reddy, D.H.K.; Kumar, B.N.; Seshaiah, K.; Rao, G.P.C.; Lu, C. Adsorption of Pb(II) from Aqueous Solutions by Chemically Modified Zeolite supported Carbon Nanotubes: Equilibrium, Kinetic, and Thermodynamic Studies. *Sep. Sci. Technol.* **2013**, *48*, 403–412. [CrossRef]
3. Assi, M.A.; Hezmee, M.N.M.; Haron, A.W.; Sabri, M.Y.M.; Rajion, M.A. The detrimental effects of lead on human and animal health. *Veter World* **2016**, *9*, 660–671. [CrossRef]
4. Rousseau, M.-C.; Straif, K.; Siemiatycki, J. IARC Carcinogen Update. *Environ. Health Perspect.* **2005**, *113*, 580. [CrossRef]
5. Gaetke, L.M.; Chow-Johnson, H.S.; Chow, C.K. Copper: Toxicological relevance and mechanisms. *Arch. Toxicol.* **2014**, *88*, 1929–1938. [CrossRef] [PubMed]
6. Larous, S.; Meniai, A.-H.; Lehocine, M.B. Experimental study of the removal of copper from aqueous solutions by adsorption using sawdust. *Desalination* **2005**, *185*, 483–490. [CrossRef]
7. Araya, M.; Olivares, M.; Pizarro, F. Copper in human health. *Int. J. Environ. Health* **2007**, *1*, 608. [CrossRef]
8. UNEP. *Global Drinking Water Quality Index Development and Sensitivity Analysis Report*; United Nations Environment Programme: Geneva, Switzerland, 2007.
9. The, U.S. Environmental Protection Agency. *Lead and Copper Rule for Drinking Water, Drinking Water Requirements for States and Public Water Systems*; USEPA: Washington, DC, USA, 2016.
10. Soliman, N.; Moustafa, A. Industrial solid waste for heavy metals adsorption features and challenges; A review. *J. Mater. Res. Technol.* **2020**, *9*, 10235–10253. [CrossRef]
11. Wieszczycka, K.; Filipowiak, K.; Wojciechowska, I.; Aksamitowski, P. Novel ionic liquid-modified polymers for highly effective adsorption of heavy metals ions. *Sep. Purif. Technol.* **2020**, *236*, 116313. [CrossRef]
12. Sandoval-Flores, G.; Alvarado-Reyna, S.; Elvir-Padilla, L.G.; Mendoza-Castillo, D.I.; Reynel-Avila, H.E.; Bonilla-Petriciolet, A. Kinetics, Thermodynamics, and Competitive Adsorption of Heavy Metals from Water Using Orange Biomass. *Water Environ. Res.* **2018**, *90*, 2114–2125. [CrossRef]
13. Ajmal, M.; Rao, R.A.K.; Ahmad, R.; Ahmad, J. Adsorption studies on *Citrus reticulata* (fruit peel of orange): Removal and recovery of Ni(II) from electroplating wastewater. *J. Hazard. Mater.* **2000**, *79*, 117–131. [CrossRef]
14. Chiban, M.; Soudani, A.; Sinan, F.; Tahrouch, S.; Persin, M. Characterization and Application of Dried Plants to Remove Heavy Metals, Nitrate, and Phosphate Ions from Industrial Wastewaters. *Clean Soil Air Water* **2011**, *39*, 376–383. [CrossRef]

15. Osman, A.I.; Ahmed, A.T.; Johnston, C.R.; Rooney, D.W. Physicochemical characterization of miscanthus and its application in heavy metals removal from wastewaters. *Environ. Prog. Sustain. Energy* **2018**, *37*, 1058–1067. [CrossRef]
16. Aman, T.; Kazi, A.A.; Sabri, M.U.; Bano, Q. Potato peels as solid waste for the removal of heavy metal copper(II) from waste water/industrial effluent. *Colloids Surf. B Biointerfaces* **2008**, *63*, 116–121. [CrossRef] [PubMed]
17. Mata, Y.; Blázquez, M.; Ballester, A.; González, F.; Muñoz, J. Sugar-beet pulp pectin gels as biosorbent for heavy metals: Preparation and determination of biosorption and desorption characteristics. *Chem. Eng. J.* **2009**, *150*, 289–301. [CrossRef]
18. Saraswat, S.K.; Demir, M.; Gosu, V. Adsorptive removal of heavy metals from industrial effluents using cow dung as the biosorbent: Kinetic and isotherm modeling. *Environ. Qual. Manag.* **2020**, *30*, 51–60. [CrossRef]
19. Joshi, N.C.; Singh, A.; Rajput, H. Utilization of Waste Leaves Biomass of Myrica Esculenta for the Removal of Pb (II), Cd (II) and Zn (II) Ions from Waste Waters. *Orient. J. Chem.* **2018**, *34*, 2548–2553. [CrossRef]
20. Czikkely, M.; Neubauer, E.; Fekete, I.; Ymeri, P.; Fogarassy, C. Review of Heavy Metal Adsorption Processes by Several Organic Matters from Wastewaters. *Water* **2018**, *10*, 1377. [CrossRef]
21. Park, J.-H.; Eom, J.-H.; Lee, S.-L.; Hwang, S.-W.; Kim, S.-H.; Kang, S.-W.; Yun, J.-J.; Cho, J.-S.; Lee, Y.-H.; Seo, D.-C. Exploration of the potential capacity of fly ash and bottom ash derived from wood pellet-based thermal power plant for heavy metal removal. *Sci. Total Environ.* **2020**, *740*, 140205. [CrossRef]
22. Qiu, R.; Cheng, F.; Huang, H. Removal of Cd2+ from aqueous solution using hydrothermally modified circulating fluidized bed fly ash resulting from coal gangue power plant. *J. Clean. Prod.* **2018**, *172*, 1918–1927. [CrossRef]
23. Mushtaq, F.; Zahid, M.; Bhatti, I.A.; Nasir, S.; Hussain, T. Possible applications of coal fly ash in wastewater treatment. *J. Environ. Manag.* **2019**, *240*, 27–46. [CrossRef]
24. Ahmaruzzaman, M. Industrial wastes as low-cost potential adsorbents for the treatment of wastewater laden with heavy metals. *Adv. Colloid Interface Sci.* **2011**, *166*, 36–59. [CrossRef]
25. Buema, G.; Harja, M.; Lupu, N.; Chiriac, H.; Forminte, L.; Ciobanu, G.; Bucur, D.; Bucur, R.D. Adsorption Performance of Modified Fly Ash for Copper Ion Removal from Aqueous Solution. *Water* **2021**, *13*, 207. [CrossRef]
26. Wu, P.; Tang, Y.; Cai, Z. Dual role of coal fly ash in copper ion adsorption followed by thermal stabilization in a spinel solid solution. *RSC Adv.* **2018**, *8*, 8805–8812. [CrossRef]
27. Kumar, M.; Goswami, L.; Singh, A.K.; Sikandar, M. Valorization of coal fired-fly ash for potential heavy metal removal from the single and multi-contaminated system. *Heliyon* **2019**, *5*, e02562. [CrossRef]
28. Xue, Q.; Li, J.-S.; Wang, P.; Liu, L.; Li, Z.-Z. Removal of Heavy Metals from Landfill Leachate Using Municipal Solid Waste Incineration Fly Ash as Adsorbent. *Clean Soil Air Water* **2014**, *42*, 1626–1631. [CrossRef]
29. Yadla, S.V.; Sridevi, V.; Chandana Lakshmi, M.V.V. Adsorption Performance of Fly Ash for the Removal of Lead. *Int. J. Eng. Res. Technol.* **2012**, *1*, 1–7.
30. Centrum Inżynierii Minerałów Antropogenicznych (Center for Engineering of Anthropogenic Minerals). Available online: http://www.cima.ibs.pw.edu.pl (accessed on 12 February 2021).
31. Filipiak, J. Wykorzystanie ubocznych produktów spalania jako stabilizatora do wzmacniania gruntów organicznych (The use of combustion by-products as a stabilizer to strengthen organic soils). *Rocz. Ochr. Sr. (Yearb. Environ. Prot.)* **2013**, *15*, 1153–1163.
32. Spalarnie Odpadów (Waste Incinerators). Available online: http://www.spalarnie-odpadow.pl (accessed on 11 February 2021).
33. World Agricultural Production. World Sunflower Production 2020/2021. Available online: http://www.worldagriculturalproduction.com/crops/sunflower.aspx (accessed on 11 January 2021).
34. Pilorgé, E. Sunflower in the global vegetable oil system: Situation, specificities and perspectives. *OCL* **2020**, *27*, 34. [CrossRef]
35. Shahbazpanahi, S.; Faraj, R.H. Feasibility study on the use of shell sunflower ash and shell pumpkin ash as supplementary cementitious materials in concrete. *J. Build. Eng.* **2020**, *30*, 101271. [CrossRef]
36. UNdata, FOASTAT, Food and Agriculture Organization, Global Roundwood Production 2019. Available online: http://data.un.org/Data.aspx?d=FAO&f=itemCode%3a1861 (accessed on 10 February 2021).
37. Tripathi, N.; Hills, C.D.; Singh, R.S.; Atkinson, C.J. Biomass waste utilisation in low-carbon products: Harnessing a major potential resource. *NPJ Clim. Atmos. Sci.* **2019**, *2*, 1–10. [CrossRef]
38. Garcia, C.A.; Hora, G. State-of-the-art of waste wood supply chain in Germany and selected European countries. *Waste Manag.* **2017**, *70*, 189–197. [CrossRef]
39. Sagar, N.A.; Pareek, S.; Sharma, S.; Yahia, E.M.; Lobo, M.G. Fruit and Vegetable Waste: Bioactive Compounds, Their Extraction, and Possible Utilization. *Compr. Rev. Food Sci. Food Saf.* **2018**, *17*, 512–531. [CrossRef]
40. Shim, Y.-S.; Kim, Y.-K.; Kong, S.-H.; Rhee, S.-W.; Lee, W.-K. The adsorption characteristics of heavy metals by various particle sizes of MSWI bottom ash. *Waste Manag.* **2003**, *23*, 851–857. [CrossRef]
41. Police, S.; Maity, S.; Chaudhary, D.K.; Dusane, C.K.; Sahu, S.K.; Kumar, A.V. Effect of coal fly ash's particle size on U adsorption in water samples and thermodynamic study on adsorption. *Environ. Chem. Ecotoxicol.* **2020**, *2*, 32–38. [CrossRef]
42. Itskos, G.; Koukouzas, N.; Vasilatos, C.; Megremi, I.; Moutsatsou, A. Comparative uptake study of toxic elements from aqueous media by the different particle-size-fractions of fly ash. *J. Hazard. Mater.* **2010**, *183*, 787–792. [CrossRef] [PubMed]
43. Lanzerstorfer, C. Fly ash from coal combustion: Dependence of the concentration of various elements on the particle size. *Fuel* **2018**, *228*, 263–271. [CrossRef]
44. Kara, S.; Aydiner, C.; Demirbas, E.; Kobya, M.; Dizge, N. Modeling the effects of adsorbent dose and particle size on the ad-sorption of reactive textile dyes by fly ash. *Desalination* **2007**, *212*, 282–293. [CrossRef]

45. Kalak, T.; Kłopotek, A.; Cierpiszewski, R. Effective adsorption of lead ions using fly ash obtained in the novel circulating flu-idized bed combustion technology. *Microchem. J.* **2019**, *145*, 1011–1025.
46. Kalak, T.; Cierpiszewski, R. Comparative studies on the adsorption of Pb(II) ions by fly ash and slag obtained from CFBC technology. *Pol. J. Chem. Technol.* **2019**, *21*, 72–81. [CrossRef]
47. Señas, L.; Priano, C.; Marfil, S.; Maiza, P.; Valea, J. Final Disposal of Ashes from Sunflower Husk in Cementitious Mortars. *Eur. J. Sci. Res.* **2012**, *74*, 292–300.
48. Brännvall, E.; Andreas, L.; Sjöblom, R.; Diener, S.; Lagerkvist, A. Factors Influencing Chemical and Mineralogical Changes in RDF Fly Ashes during Aging. *J. Environ. Eng.* **2014**, *140*, 04013014. [CrossRef]
49. Sevim, O.; Demir, I. Particle Size Optimization of Fly Ash. *Int. J. Adv. Mech. Civ. Eng.* **2017**, *4*, 85–87.
50. Nnaji, C.C.; Emefu, S.C. Effect of Particle Size on the Sorption of Lead from Water by Different Species of Sawdust: Equilibrium and Kinetic Study. *Bioresources* **2017**, *12*, 4123–4145. [CrossRef]
51. Kumar, S.; Singh, J.; Mohapatra, S.K. Influence of Particle Size on Leaching characteristic of fly ash. In Proceedings of the 15th International Conference on Environmental Science and Technology, Rhodes, Greece, 31 August–2 September 2017; pp. 1–7.
52. Dos Santos, R.P.; Martins, J.; Gadelha, C.; Cavada, B.; Albertini, A.V.; Arruda, F.; Vasconcelos, M.; Teixeira, E.; Alves, F.; Filho, J.L.; et al. Coal Fly Ash Ceramics: Preparation, Characterization, and Use in the Hydrolysis of Sucrose. *Sci. World J.* **2014**, *2014*, 1–7. [CrossRef] [PubMed]
53. Paya, J.; Monzo, J.; Borrachero, M.V.; Perris, E.; Amahjour, F. Thermogravimetric methods for determinig carbon content in fly ashes. *Cem. Concr. Res.* **1998**, *28*, 675–686. [CrossRef]
54. Kim, T.; Olek, J. Effects of Sample Preparation and Interpretation of Thermogravimetric Curves on Calcium Hydroxide in Hydrated Pastes and Mortars. *Transp. Res. Rec. J. Transp. Res. Board* **2012**, *2290*, 10–18. [CrossRef]
55. Zhou, Z.; Sofi, M.; Lumantarna, E.; san Nicolas, R.; Hadi, K.G.; Mendis, P. Strength Development and Thermogravimetric Investigation of High-Volume Fly Ash Binders. *Materials* **2019**, *12*, 3344. [CrossRef]
56. López-Maldonado, E.A.; Oropeza-Guzmán, M.T. Strategic Design of Heavy Metals Removal Agents through Zeta Potential Measurements. In *Heavy Metals*; Saleh, H.E.-D.M., Aglan, R.F., Eds.; InTechOpen: London, UK, 2018.
57. Cherian, C.; Siddiqua, S. Pulp and Paper Mill Fly Ash: A Review. *Sustainability* **2019**, *11*, 4394. [CrossRef]
58. Topini, D.; Toraldo, E.; Andena, L.; Mariani, E. Use of recycled fillers in bituminous mixtures for road pavements. *Constr. Build. Mater.* **2018**, *159*, 189–197. [CrossRef]
59. Silva, R.; de Brito, J.; Lynn, C.; Dhir, R. Environmental impacts of the use of bottom ashes from municipal solid waste incineration: A review. *Resour. Conserv. Recycl.* **2019**, *140*, 23–35. [CrossRef]
60. Bansal, R.C.; Goyal, M. *Activated Carbon Adsorption*; CRC Press, Taylor and Francis Group, LLC: Boca Raton, FL, USA, 2005.
61. Li, X.; Gao, Z.; Fang, S.; Ren, C.; Yang, K.; Wang, F. Fractal Characterization of Nanopore Structure in Shale, Tight Sandstone and Mudstone from the Ordos Basin of China Using Nitrogen Adsorption. *Energies* **2019**, *12*, 583. [CrossRef]
62. Horikawa, T.; Do, D.; Nicholson, D. Capillary condensation of adsorbates in porous materials. *Adv. Colloid Interface Sci.* **2011**, *169*, 40–58. [CrossRef]
63. Weng, C.-H.; Huang, C. Adsorption characteristics of Zn(II) from dilute aqueous solution by fly ash. *Colloids Surf. A Physicochem. Eng. Asp.* **2004**, *247*, 137–143. [CrossRef]
64. Mroczek, K.; Kalisz, S.; Pronobis, M.; Sołtys, J. The effect of halloysite additive on operation of boilers firing agricultural biomass. *Fuel Process. Technol.* **2011**, *92*, 845–855. [CrossRef]
65. Gao, J.; Wang, T.; Zhao, J.; Hu, X.; Dong, C. An Experimental Study on the Melting Solidification of Municipal Solid Waste Incineration Fly Ash. *Sustain. J. Rec.* **2021**, *13*, 535. [CrossRef]
66. Bada, S.O.; Potgieter-Vermaak, S. Evaluation and Treatment of Coal Fly Ash for Adsorption Application. *Leonardo Electron. J. Pract. Technol.* **2008**, *12*, 37–48.
67. Farghali, A.; Bahgat, M.; Allah, A.E.; Khedr, M. Adsorption of Pb(II) ions from aqueous solutions using copper oxide nanostructures. *Beni Suef Univ. J. Basic Appl. Sci.* **2013**, *2*, 61–71. [CrossRef]
68. Franus, M.; Bandura, L. Sorption of heavy metal ions from aqueous solution by glauconite. *Fresenius Environ. Bull.* **2014**, *23*, 825–839.
69. Cuppett, J.D.; Duncan, S.E.; Dietrich, A.M. Evaluation of Copper Speciation and Water Quality Factors That Affect Aqueous Copper Tasting Response. *Chem. Senses* **2006**, *31*, 689–697. [CrossRef] [PubMed]
70. Escudero, R.; Espinoza, E.; Tavera, F.J. Precipitation of Lead Species in a Pb—$H_2O$ System. *Res. J. Recent Sci.* **2013**, *2*, 1–8.
71. Lee, J.-Y.; Chen, C.H.; Cheng, S.; Li, H.-Y. Adsorption of Pb(II) and Cu(II) metal ions on functionalized large-pore mesoporous silica. *Int. J. Environ. Sci. Technol.* **2016**, *13*, 65–76. [CrossRef]
72. Darmayanti, L.; Notodarmodjo, S.; Damanhuri, E. Removal of Copper (II) Ions in Aqueous Solutions by Sorption onto Fly Ash. *J. Eng. Technol. Sci.* **2017**, *49*, 546. [CrossRef]
73. Kobayashi, Y.; Ogata, F.; Saenjum, C.; Nakamura, T.; Kawasaki, N. Removal of $Pb^{2+}$ from Aqueous Solutions Using K-Type Zeolite Synthesized from Coal Fly Ash. *Water* **2020**, *12*, 2375. [CrossRef]
74. Vu, N.H.; Kristianová, E.; Dvořák, P.; Abramowski, T.; Dreiseitl, I.; Adrysheva, A. Modified Leach Residues from Processing Deep-Sea Nodules as Effective Heavy Metals Adsorbents. *Metals* **2019**, *9*, 472. [CrossRef]
75. Cui, X.; Fang, S.; Yao, Y.; Li, T.; Ni, Q.; Yang, X.; He, Z. Potential mechanisms of cadmium removal from aqueous solution by Canna indica derived biochar. *Sci. Total Environ.* **2016**, *562*, 517–525. [CrossRef]

76. Mishra, A.; Tripathi, B.D. Utilization of fly ash in adsorption of heavy metals from wastewater. *Toxicol. Environ. Chem.* **2008**, *90*, 1091–1097. [CrossRef]
77. Sočo, E.; Kalembkiewicz, J. Comparison of adsorption of Cd(II) and Pb(II) ions on pure and chemically modified fly ashes. *Chem. Process. Eng.* **2016**, *37*, 215–234. [CrossRef]
78. Harja, M.; Buema, G.; Lupu, N.; Chiriac, H.; Herea, D.D.; Ciobanu, G. Fly Ash Coated with Magnetic Materials: Improved Adsorbent for Cu (II) Removal from Wastewater. *Materials* **2020**, *14*, 63. [CrossRef]
79. Militaru, B.A.; Pode, R.; Lupa, L.; Schmidt, W.; Tekle-Röttering, A.; Kazamer, N. Using Sewage Sludge Ash as an Efficient Adsorbent for Pb (II) and Cu (II) in Single and Binary Systems. *Molecules* **2020**, *25*, 2559. [CrossRef]
80. Igberase, E.; Osifo, P.; Ofomaja, A. The Adsorption of Pb, Zn, Cu, Ni, and Cd by Modified Ligand in a Single Component Aqueous Solution: Equilibrium, Kinetic, Thermodynamic, and Desorption Studies. *Int. J. Anal. Chem.* **2017**, *2017*, 1–15. [CrossRef] [PubMed]
81. Zaranyika, M.F.; Chirinda, T. Heavy metal speciation trends in mine slime dams: A case study of slime dams at a goldmine in Zimbabwe. *J. Environ. Chem. Ecotoxicol.* **2011**, *3*, 103–115.
82. Igwe, J.; Abia, A. Adsorption isotherm studies of Cd (II), Pb (II) and Zn (II) ions bioremediation from aqueous solution using unmodified and EDTA-modified maize cob. *Eclética Química J.* **2007**, *32*, 33–42. [CrossRef]
83. Kalak, T.; Dudczak-Hałabuda, J.; Tachibana, Y.; Cierpiszewski, R. Effective use of elderberry (*Sambucus nigra*) pomace in biosorption processes of Fe(III) ions. *Chemosphere* **2020**, *246*, 125744. [CrossRef] [PubMed]
84. Esmaeili, H.; Foroutan, R. Investigation into ion exchange and adsorption methods for removing heavy metals from aqueous solution. *Int. J. Biol. Pharm. Allied Sci.* **2015**, *4*, 620–629, ISSN: 2277–4998.
85. Hałas, P.; Kołodyńska, D.; Płaza, A.; Gęca, M.; Hubicki, Z. Modified fly ash and zeolites as an effective adsorbent for metal ions from aqueous solution. *Adsorpt. Sci. Technol.* **2017**, *35*, 519–533. [CrossRef]
86. Alinnor, I. Adsorption of heavy metal ions from aqueous solution by fly ash. *Fuel* **2007**, *86*, 853–857. [CrossRef]
87. Ofomaja, A.E.; Naidoo, E.B.; Modise, S.J. Kinetic and Pseudo-Second-Order Modeling of Lead Biosorption onto Pine Cone Powder. *Ind. Eng. Chem. Res.* **2010**, *49*, 2562–2572. [CrossRef]
88. Kalembkiewicz, J.; Galas, D.; Sitarz-Palczak, E. The Physicochemical Properties and Composition of Biomass Ash and Evalu-ating Directions of its Applications. *Pol. J. Environ. Stud.* **2018**, *27*, 2593–2603. [CrossRef]